2014 IEEE International Conference on Robotics & Automation (ICRA)
Hong Kong Convention and Exhibition Center
May 31 - June 7, 2014. Hong Kong, China

Personal Robot Assisting Transportation to Support Active Human Life

– Reference Generation based on Model Predictive Control for Robust Quick Turning–

Noriaki Hirose[1], Ryosuke Tajima[1], Kazutoshi Sukigara[1], and Minoru Tanaka[1]

***Abstract*— Various robots are being developed to support active human lifestyles throughout the world. In particular, robots that can support a comfortable lifestyle for elderly people are needed for the coming super-aging society in many countries. The authors have already proposed the Personal Robot (PR) shown in Fig. 1, which can follow a human being and carry their baggage; the PR user does not need to carry heavy bags, even after shopping. The PR, therefore, can encourage not only elderly people but also young people to walk outside . This means that the PR can support a life of wellness in the true sense. In conventional research, a control approach for the roll angle is proposed to ensure the stability margin for steady turning because in order to follow a human being, the PR must realize high traveling performance.**

In this paper, a method of reference generation for the roll angle and turning angular velocity is proposed to take into account the stability margin during the transient state using model predictive control. According to the proposed approach, the quickest turning motion can be realized by keeping the upper and lower boundary constraints for the zero moment point (ZMP). The effectiveness of the proposed approach is verified by experiment using the prototype PR.

I. INTRODUCTION

Various robots are being developed to support active human lifestyles throughout the world [1][2][3]. In particular, robots that can support a comfortable life for elderly people are needed for the coming super-aging society in many countries. However, robots that provide excessive or premature support to elderly people may actually cause their physical ability to decline sooner. The authors have already proposed the Personal Robot (PR) shown in Fig. 1 [4], which can follow a human being and carry their baggage [5]. The PR user does not need to carry heavy bags, even after shopping. The PR, therefore, can encourage not only elderly people but also young people to walk outside . This means that the PR can support a life of wellness in the true sense.

In order to follow the human being, the PR requires a high traveling performance like that of a human being. In addition, the footprint of the PR has to be small to coexist in society. However, the small footprint results in a higher center of gravity, which deteriorates the traveling performance. Therefore, it is difficult for the PR to realize both high traveling performance and a small footprint. The authors proposed the use an actuator to control the roll angle (posture actuator) of the PR [4][6][7][8][9]. In conventional research [4], the control approach for the roll angle using

[1]N. Hirose, R. Tajima, and K. Sukigara are with Intelligent Systems Lab., Information & Electronics Research Div., Toyota Central R & D Labs., Inc., 41-1 Yokomichi Nagakute Aichi JAPAN hirose at mosk.tytlabs.co.jp

[a] front view [b] following human being

Fig. 1. Overview of Personal Robot.

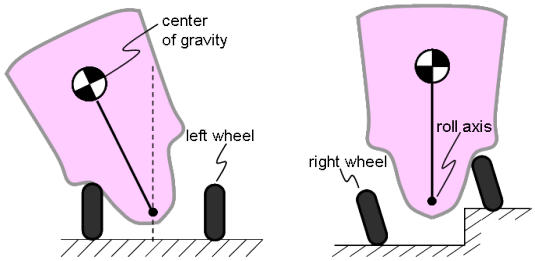

[a] turning [b] uneven floor

Fig. 2. Target behavior of PR for roll axis.

the lateral acceleration is applied to realize a appropriate tilting posture during steady turning motion and a vertical posture, even on an uneven road surface, as shown in Fig. 2. And, the previous work shown in [6] proposes the feedback compensation with the unstable pole to realize the desired posture during the steady state by zeroing the control input of the posture actuator. However, these conventional approaches don't take into account stability margin at the transient state of the turning motion, although the desired posture in the steady state can be achieved. Therefore, the PR loses the stability margin and falls during the transient state, which represents the transition from going straight ahead to steady turning or from steady turning to going straight ahead.

In this paper, a method of reference generation for the roll angle and turning angular velocity is proposed to take into account the stability margin at the transient state using model predictive control [10][11][12]. Moreover, the proposed approach also can consider the saturation of the posture actuator torque and the suppression of discontinuity for practical use. According to the proposed approach, the quickest turning motion can be realized under keeping the constraints of the upper and lower boundaries for the zero moment point (ZMP). The effectiveness of the proposed

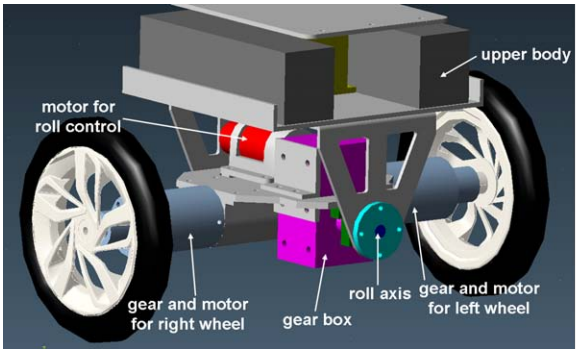

[a] 3D drawing sheet

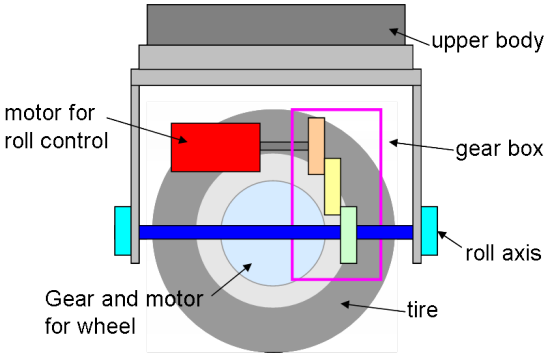

[b] lateral view

Fig. 3. Structure for posture actuator.

approach is verified by experiments using the prototype PR.

II. PROTOTYPE OF PERSONAL ROBOT

In this section, the mechanical system of the PR and the whole control system are explained before designing the proposed approach. And, the conventional approach ignoring the transient state is shown for the comparison.

A. Mechanical System

Figure 3 shows the mechanical structure of the PR. Fig. 3[a] is a 3D view of the drawing sheets, and [b] is a simplified lateral-view diagram. The PR has two driving wheels to realize stabilization of the pitch angle and the desired traveling velocity by wheeled inverted pendulum control [13][14]. In addition, the turning angular velocity can be controlled by giving a difference in the rotation speed between the right and left wheels. On the other hand, a posture actuator with a motor and gear is used to achieve tilting of the upper body for quick turning and a vertical posture, even on a slope [6]. The posture actuator is driven by the control method using the lateral acceleration for the realization of the stable posture [4].

B. Control System

Figure 4 shows a block diagram of the proposed control system for the prototype PR. Here, v_{ref} and ω_{refc} are the references for the traveling velocity v and the turning angular velocity ω (which are generated by the upper process

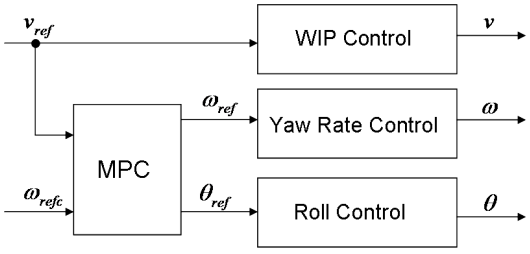

Fig. 4. Block diagram of control system for PR.

for following the human being [15]), ω_{ref} is the modified reference for the turning angular velocity by model predictive control, and θ_{ref} is the reference for the roll angle θ (which is generated by model predictive control). In addition, "WIP Control" is the wheeled inverted pendulum control system (which controls the pitch angle and the traveling velocity v to realize the desired value v_{ref}), "Yaw Rate Control" is the feedback control system (which controls the turning angular velocity ω), "Roll control" is the two-degree-of-freedom control system with feedback and feedforward compensation[16] for the roll angle θ using the lateral acceleration [4], and "MPC" is the proposed algorithm (which can generate the modified reference ω_{ref} and the appropriate reference of the roll angle θ_{ref} to keep the prescribed stability margin). In order to take into account the stability margin in the "MPC," the ZMP equation should be formulated.

C. ZMP Equation of PR

Figure 5 shows a rear view of the PR model. Here, J is the inertia of the upper body, M is the weight of the upper body, h is the distance between the center of gravity and the roll axis, r is the radius of the wheel, p is the position of the center of gravity, and q is the position of the ZMP. The following equation is the ZMP equation for the $Y-Z$ axis:

$$-(p_y - q_y)f_z + (p_z - q_z)f_y = J\ddot{\theta} \tag{1}$$

Here, p_y, p_z, q_z, f_y, and f_z can be shown as follows:

$$\begin{aligned} p_y &= -h\sin\theta, \\ p_z &= h\cos\theta + r, \\ q_z &= 0, \\ f_y &= M(v\omega + h\omega^2\sin\theta - h\ddot{\theta}\cos\theta), \\ f_z &= M(g - h\ddot{\theta}\sin\theta), \end{aligned} \tag{2}$$

where g is the gravity acceleration. By substituting (2) into (1), the ZMP trajectory q_y for the y axis can be obtained as follows:

$$\begin{aligned} q_y = &-\frac{(v\omega + h\omega^2\sin\theta - h\ddot{\theta}\cos\theta)(h\cos\theta + r)}{g - h\ddot{\theta}\sin\theta} \\ &-h\sin\theta + \frac{J\ddot{\theta}}{M(g - h\ddot{\theta}\sin\theta)}. \end{aligned} \tag{3}$$

(3) can be simplified by substituting $\sin\theta = \theta$, $\cos\theta = 1$, and $h\ddot{\theta}\sin\theta = 0$ under the assumption that $\theta \ll 1$ and $g \gg$

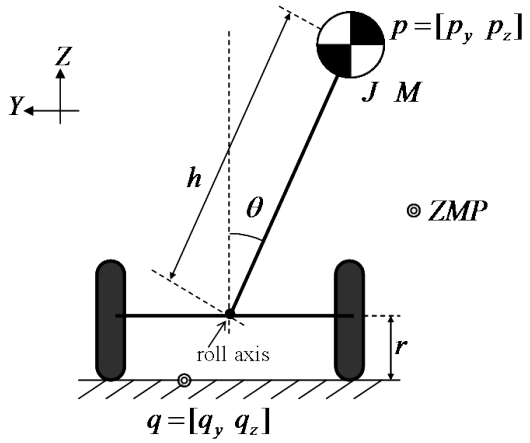

Fig. 5. Model of personal robot for roll axis.

$h\ddot{\theta}\sin\theta$.

$$q_y = -\frac{(h+r)v}{g}\omega + \frac{h(h+r)+\frac{J}{M}}{g}\ddot{\theta} - (h+\frac{(h+r)h\omega^2}{g})\theta \quad (4)$$

In the conventional approach not considering $\ddot{\theta}$, the following reference θ_{ref} is generated by substituting $\ddot{\theta}=0$, $q_y=0$, $v=v_{ref}$, and $\omega=\omega_{ref}$ into (4), only to realize the most stable posture $q_y=0$ at steady turning:

$$\theta_{ref} = -\frac{v_{ref}\omega_{ref}}{\frac{h}{h+r}g + h\omega_{ref}^2} \quad (5)$$

Here, v_{ref} and ω_{ref} are used for θ_{ref} in (5) instead of the actual values v and ω. According to (5), the conventional approach generates θ_{ref} for not only steady state but also the transient state. Therefore, the conventional approach has problems at the transient state. For example, if $\ddot{\omega}_{ref}$ has a large value to realize quick turning during the steady traveling velocity, a large amount of angular acceleration $\ddot{\theta}$ is occurred. It is obvious from the second derivative of (5). As a result, the ZMP trajectory q_y in (3) exceeds the desired range during the transient state. It means that the PR loses the stability margin and may fall in some situations. In the conventional approach, the conservative reference ω_{ref} to suppress $\ddot{\omega}_{ref}$ has to be applied to ensure posture stabilization. The desired quick turning, therefore, cannot be achieved in the conventional approach.

III. REFERENCE GENERATION BY MODEL PREDICTIVE CONTROL

In the proposed control system, model predictive control is applied to generate the reference of the roll angle θ_{ref} and the reference of the turning angular velocity ω_{ref}. The model predictive control approach can take into account the inequality constraints for the predicted future values [10]. The ZMP trajectory q_y, therefore, can be limited to within upper and lower boundaries. In addition, ω_{ref} can converge quickly to the target value ω_{refc} to realize quick turning within the desired range of the ZMP.

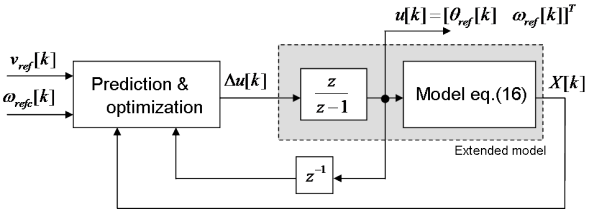

Fig. 6. Block diagram for the proposed model predictive control approach.

Figure 6 shows a block diagram of the proposed approach, which corresponds to the "MPC" shown in Fig. 4. In this section, at first, the conditions for the design of the model predictive control are shown in III-A. Next, the mathematical model is designed to formulate the model predictive control in III-B, and the method of prediction and optimization for generating θ_{ref} and ω_{ref} is shown in III-C.

A. Conditions for Model Predictive Control

The following factors should be considered when designing the model predictive control for practical use:

i) limitation of the ZMP q_y
ii) limitation of the roll angle θ
iii) limitation of the actuator torque τ
iv) attenuation of the error between ω_{refc} and ω_{ref}
v) suppression of the jerk j_x around the x axis
vi) suppression of the discontinuity for the references θ_{ref} and ω_{ref}

The proposed approach gives the upper and lower boundaries for i), ii), and iii) as inequality constraints. In addition, i), iii), iv), v), and vi) are taken into account by the minimization of the evaluation function. Also, v) and vi) are required to implement model predictive control in the experiment to avoid unknown phenomena in the higher frequency range.

B. Predictive Model

The roll control system indicated in Fig. 4 as "Roll Control" is designed as the following third-order system, assuming there are no disturbance forces and no perturbations in the plant system:

$$\theta = \frac{\omega_r^2}{s^2+2\zeta_r\omega_r s+\omega_r^2}\cdot\frac{\omega_r}{s+\omega_r}\theta_{ref}, \quad (6)$$

where ω_r is $2\times\pi\times 2.0$, and ζ_r is 0.95. Then, (6) can be transformed into the following state space expression:

$$\frac{d}{dt}\begin{bmatrix}\ddot{\theta}\\ \dot{\theta}\\ \theta\end{bmatrix} = \begin{bmatrix}a_{r1} & a_{r2} & a_{r3}\\ 1 & 0 & 0\\ 0 & 1 & 0\end{bmatrix}\begin{bmatrix}\ddot{\theta}\\ \dot{\theta}\\ \theta\end{bmatrix} + \begin{bmatrix}b_r\\ 0\\ 0\end{bmatrix}\theta_{ref}, \quad (7)$$

where $a_{r1} = -2\zeta_r\omega_r - \omega_r$, $a_{r2} = -\omega_r^2 - 2\zeta_r\omega_r^2$, $a_{r3} = -\omega_r^3$, and $b_r = \omega_r^3$. (7) can be discretized by the zero-order-hold method as follows:

$$x_r[k+1] = A_r x_r[k] + B_r \theta_{ref}[k], \tag{8}$$

where A_r and B_r are the state space matrices, and x_r is the following state matrix:

$$x_r[k] = \left[\begin{array}{ccc} \ddot{\theta}[k] & \dot{\theta}[k] & \theta[k] \end{array} \right]^T. \tag{9}$$

On the other hand, the "Yaw Rate Control" shown in Fig. 4 can realize a higher control bandwidth than the roll control system to achieve the precise human following. Its control system, therefore, can be approximated as a delay of one step.

$$\omega[k] = \omega_{ref}[k-1] \tag{10}$$

By combining (8) and (10) and adding the $\ddot{\theta}[k-1]$ to deal with the jerk j_x, the following model can be generated:

$$\left[\begin{array}{c} x_r[k+1] \\ \ddot{\theta}[k] \\ \omega_{ref}[k] \end{array} \right] = \left[\begin{array}{ccc} A_r & 0 & 0 \\ A_{r1} & 0 & 0 \\ 0 & 0 & 0 \end{array} \right] \cdot \left[\begin{array}{c} x_r[k] \\ \ddot{\theta}[k-1] \\ \omega_{ref}[k-1] \end{array} \right] + \left[\begin{array}{cc} B_r & 0 \\ 0 & 0 \\ 0 & 1 \end{array} \right] \left[\begin{array}{c} \theta_{ref}[k] \\ \omega_{ref}[k] \end{array} \right], \tag{11}$$

where $A_{r1} = [1 \ 0 \ 0]$. (11) can be redefined as follows to simplify the after-mentioned formulation:

$$X[k+1] = AX[k] + Bu[k]. \tag{12}$$

In order to take into account the ZMP trajectory q_y for i), the actuator torque τ for iii), the turning angular velocity ω for iv), and the jerk j_x for v) in the evaluation function, the output equation can be generated as follows by (10), (26), (28) and (29) shown in appendix:

$$\left[\begin{array}{c} q_y[k] \\ \tau[k] \\ \omega[k] \\ j_x[k] \end{array} \right] = \left[\begin{array}{ccccc} c_1 & 0 & c_2 & 0 & c_3 \\ c_4 & 0 & c_5 & 0 & c_6 \\ 0 & 0 & 0 & 0 & 1 \\ 1 & 0 & 0 & -1 & 0 \end{array} \right] X[k], \tag{13}$$

where c_1, c_2, c_3, c_4, c_5, and c_6 can be described as follows:

$$\begin{aligned} c_1 &= \frac{h(h+r) + \frac{J}{M}}{g}, \\ c_2 &= -h - \frac{(h+r)h\omega_{ref}^2}{g}, \\ c_3 &= -\frac{(h+r)v_{ref}}{g}, \\ c_4 &= J + Mh^2, \\ c_5 &= -hMg - h^2 M\omega_{ref}^2, \\ c_6 &= -hMv_{ref}. \end{aligned} \tag{14}$$

(13) can then be redefined as follows:

$$z[k] = CX[k]. \tag{15}$$

On the other hand, the discrete integration $\frac{z}{z-1}$ is added to the control input $u(k)$ in order to consider vi) [17] as shown in Fig. 6. The following input $\Delta u[k]$ is given as the control input to the extended model with $\frac{z}{z-1}$.

$$\Delta u[k] = u[k] - u[k-1] \tag{16}$$

C. Formulation of Model Predictive Control

The "prediction & optimization" shown in Fig. 6 calculates $\Delta u[k]$ by solving the following quadratic programming problem with inequality constraints:

$$\begin{aligned} \min_{\Delta U[k]} \quad & V[k] = (R[k] - Z[k])^T Q (R[k] - Z[k]) \\ & \qquad + \Delta U[k]^T W \Delta U[k], && (17) \\ \text{subject to} \quad & q_{ymin} \le Q_y[k] \le q_{ymax}, && (18) \\ & \tau_{min} \le T[k] \le \tau_{max}, && (19) \\ & \theta_{min} \le \Theta_{ref}[k] \le \theta_{max}, && (20) \end{aligned}$$

where $R[k]$, $Z[k]$, $\Delta U[k]$, $Q_y[k]$, $T[k]$, and $\Theta_{ref}[k]$ are shown as follows:

$$\begin{aligned} R[k] &= [r(k+1|k) \ \ldots \ r(k+N_p|k)]^T, \\ Z[k] &= [\hat{z}(k+1|k) \ \ldots \ \hat{z}(k+N_p|k)]^T, \\ \Delta U[k] &= [\Delta\hat{u}(k|k) \ \ldots \ \Delta\hat{u}(k+N_u-1|k)]^T, \\ Q_y[k] &= [\hat{q}_y(k+1|k) \ \ldots \ \hat{q}_y(k+N_p|k)]^T, \\ T[k] &= [\hat{\tau}(k+1|k) \ \ldots \ \hat{\tau}(k+N_p|k)]^T, \\ \Theta_{ref}[k] &= [\hat{\theta}_{ref}(k+1|k) \ \ldots \ \hat{\theta}_{ref}(k+N_u|k)]^T, \end{aligned} \tag{21}$$

and where N_p is the number of steps for the prediction, N_u is the number of control inputs generated in each sampling period, and $r(k+i|k)(i = 1, \ldots, N_p)$ represents the following constant vector for the reference:

$$\begin{aligned} & r(k+1|k) = \ldots \\ & \ldots = r(k+N_p|k) = [0 \ \ 0 \ \ \omega_{refc}[k] \ \ 0]^T \end{aligned} \tag{22}$$

In addition, Q and W are the weight matrices, q_{ymin}, q_{ymax}, τ_{min}, and τ_{max} are the $N_p \times 1$ constant matrices (which give the upper and lower boundaries for q_y and τ), θ_{min}, and θ_{max} are the $N_u \times 1$ constant matrices (which give the boundary for θ_{ref}) . According to the appendix, $V[k]$ can be transformed into the quadratic form of $\Delta U[k]$. Also, the inequalities shown in (18), (19), and (20) can be redefined as the linear inequalities of $\Delta U[k]$. Therefore, $\Delta U[k]$, which minimizes $V[k]$ in (17) with the inequality constraints (18), (19), and (20), can be calculated by solving the quadratic programming problem [10]. As a result, the control input $\Delta u[k]$ shown in Fig. 6 can be given as follows at the k-th step:

$$\Delta u[k] = \Delta\hat{u}(k|k). \tag{23}$$

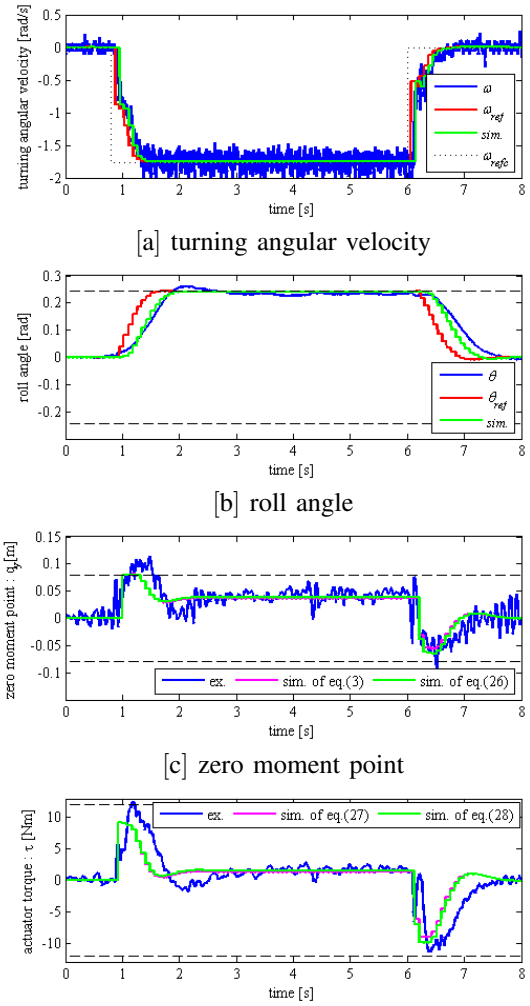

[a] turning angular velocity

[b] roll angle

[c] zero moment point

[d] actuator torque

Fig. 7. Experimental results. (v_{ref} = 1.667 [m/s], ω_{refc} = 1.766 [rad/s])

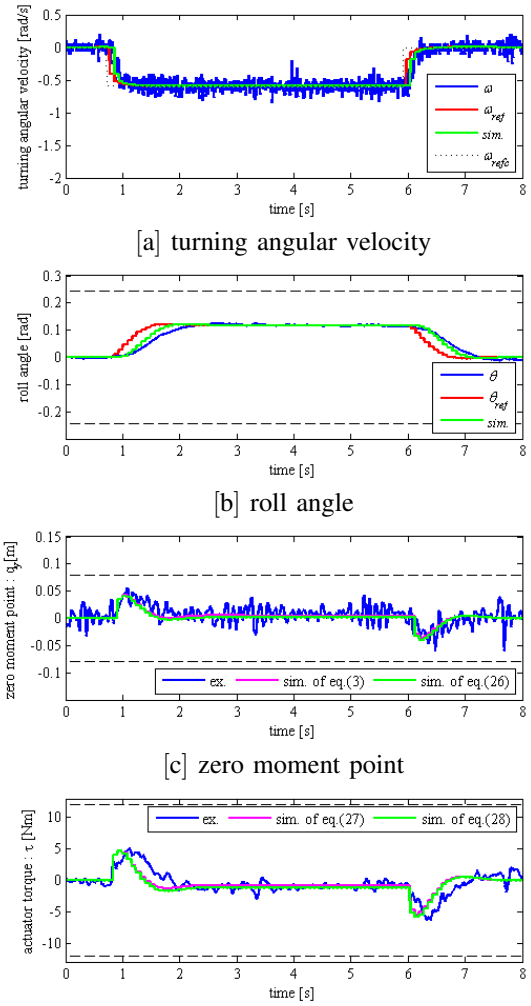

[a] turning angular velocity

[b] roll angle

[c] zero moment point

[d] actuator torque

Fig. 8. Experimental results. (v_{ref} = 1.667 [m/s], ω_{refc} = 0.5886 [rad/s])

IV. EXPERIMENTAL RESULTS

Several times of experiments are performed to verify the effectiveness and repeatability of the proposed approach. In the experiment, the references of the turning angular velocity ω_{refc} = 1.766 rad/s and 0.588 rad/s are given to the PR at the traveling velocity $v_{ref} = v$ = 1.667 m/s. On the other hand, the calculation of the quadratic programming problem is implemented into the MicroAutoBox – dSPACE by using Matlab/Simulink to generate the $\Delta u[k]$ at the sampling period T_s = 80 ms.

A. Parameters for Model Predictive Control

The weighting matrix Q is designed as follows by trial and error to stabilize the model predictive control system:

$$Q = \begin{bmatrix} Q_{opt} & \cdots & 0 & 0 \\ \vdots & \ddots & \vdots & \vdots \\ 0 & \cdots & Q_{opt} & 0 \\ 0 & \cdots & 0 & Q_{optf} \end{bmatrix}, \quad (24)$$

where Q_{opt} and Q_{optf} are designed as follows:

$$\begin{aligned} Q_{opt} &= \mathrm{diag}\left[\begin{array}{cccc} 10 & 20 & 0.01 & 30 \end{array}\right], \\ Q_{optf} &= \mathrm{diag}\left[\begin{array}{cccc} 10^5 & 20 & 0.01 & 30 \end{array}\right]. \end{aligned} \quad (25)$$

On the other hand, another weighting matrix W is designed as the unit matrix $2 \cdot N_u \times 2 \cdot N_u$ to suppress the discontinuity of $U[k]$. The other free parameters for model predictive control are listed in Table I.

B. Experimental Results

Figure 7 shows the experimental results for the turning motion ω_{refc} = 1.766 rad/s at the traveling velocity v_{ref} = 1.667 m/s. The centripetal acceleration during this turning motion corresponds to $0.3 \times g$, which is the maximum value for the specification of the prototype PR. Fig. 7[a] indicates the turning angular velocity, [b] indicates the roll angle, [c] indicates the calculated zero moment point by (26), and [d] indicates the actuator torque. In all of the figures, the blue lines show the actual responses in the experiment, the green lines show the responses in the simulation, and the

horizontal broken lines show the upper and lower boundaries from the model predictive control. In addition, the simulation responses without linear approximation are shown as the magenta lines in Fig.7[c] and [d]. In Fig. 7[a], the red line shows the reference ω_{ref} generated by the proposed approach, and the dotted black line shows the reference ω_{refc}. In Fig. 7[b], the red line shows the reference θ_{ref} generated by the proposed approach.

From Fig. 7[b], [c], and [d], the roll angle, the ZMP, and the actuator torque can be successfully limited by the desired upper and lower boundaries in both the experiment and the simulation. The quick turning motion can be confirmed in Fig. 7[a] under the above limitations. The reaching times to 50% and 90% of ω_{refc} are 0.16 s and 0.46 s, respectively. In addition, the suppression of the discontinuity for θ_{ref} and ω_{ref} are also verified from Fig. 7[a] and [b]. On the other hand, the experimental responses approximately coincide with the responses in the simulation, although there is a small difference between the experiment and the simulation caused by the perturbation of the model, the disturbance in the experiment, and the sensor noise. And, from Fig.7[c] and [d], the green lines with linearization coincide well with the magenta lines without linearization. It means that the validity of the linear approximation approach shown in appendix A can be proved.

Figure 8 shows the experimental results for the turning motion ω_{refc} = 0.588 rad/s at the traveling velocity v_{ref} = 1.667 m/s. The centripetal acceleration during steady turning corresponds to 0.1 $\times g$. From Fig. 8[a], a faster response is realized compared to that in Fig. 7[a]. The reaching times to 50% and 90% of ω_{refc} are 0.13 s and 0.21 s, respectively. Because, the ZMP and the actuator torque have some margin against the upper and lower boundaries, as shown in Fig. 8[c] and [d]. Figs. 7 and 8 are the experimental waveforms for one trial. However, the repeatability of the proposed approach is confirmed by several experiments at same conditions.

Fig. 9 shows snapshots of the turning motion from Fig. 7. The PR tilts its upper body based on the reference of the model predictive control and achieves quick turning.

C. Simulation Results for the Conventional Approach

Figure 10 shows the simulation results for the conventional approach of (5) to realize the same performance of the turning angular velocity as in Fig. 7[a]. Fig. 10 is shown in the same manner as Fig. 7. The conventional approach actually realizes $q_y = 0$ at steady turning. However, the roll angle, the ZMP, and the actuator torque exceed the desired boundaries indicated by the horizontal broken lines. From the simulation, the merits of the proposed approach over the conventional approach are clearly presented.

V. CONCLUSION

In this paper, a reference generation approach based on model predictive control for the PR was proposed to realize quick turning under the upper and lower constraints of the ZMP and actuator torque. The proposed approach can generate the references for the roll angle and turning angular velocity to keep the desired stability margin using the inequality constraints. Moreover, model predictive control optimizes these references to suppress discontinuity of the references and to attenuate the error of the turning angular velocity by minimizing the evaluation function.

The effectiveness of the proposed approach was verified by the simulation and experiments using the prototype PR. For future work, we propose shortening the sampling period T_s by the reduction in computational load for the model predictive control and keeping the robustness for variation of baggage mass.

TABLE I

PARAMETERS FOR THE MODEL PREDICTIVE CONTROL.

weight of upper body	M [kg]	17.76
inertia of upper body	J [kg m^2]	1.12
height of center of gravity	h [m]	0.31
radius of wheel	r [m]	0.10
the number of steps for prediction	N_p	30
the number of control input	N_u	5
upper boundary of ZMP	q_{ymax} [m]	0.080
lower boundary of ZMP	q_{ymin} [m]	-0.080
upper boundary of actuator torque	τ_{max} [Nm]	12.06
lower boundary of actuator torque	τ_{min} [Nm]	-12.06
upper boudary of roll reference	θ_{max} [rad]	0.24
lower boudary of roll reference	θ_{max} [rad]	-0.24

APPENDIX

In order to solve (17), (18), (19), and (20) as the quadratic programming problem, the ZMP trajectory q_y, the actuator torque τ, and the jerk j_x are defined as the linear equation, $V[k]$ is transformed into the quadratic form of $\Delta U[k]$, and the inequalities in (18), (19), and (20) are transformed into the linear inequality of $\Delta U[k]$, respectively [10].

A. Linearization of q_y, τ, and j_x

The following linearized q_y can be generated by substituting $\omega^2 = \omega_{ref}^2$ and $v = v_{ref}$ into (4).

$$\begin{aligned} q_y &= -\frac{(h+r)v_{ref}}{g}\omega + \frac{h(h+r)+\frac{J}{M}}{g}\ddot{\theta} \\ &\quad -(h+\frac{(h+r)h\omega_{ref}^2}{g})\theta \end{aligned} \tag{26}$$

Here, ω^2 and v are assumed as the steady value among the predictive horizon N_p steps.

On the other hand, the motion equation around the roll axis can be expressed as follows:

$$\begin{aligned} (J+Mh^2)\ddot{\theta} &= \tau + hMg\sin\theta \\ &\quad +hM(v\omega+\omega^2 h\sin\theta)\cos\theta. \end{aligned} \tag{27}$$

(27) can be linearized by $\sin\theta = \theta$, $\cos\theta = 1$, $\omega^2 = \omega_{ref}^2$ and $v = v_{ref}$. As a result, the actuator torque τ can be expressed as follows:

$$\begin{aligned} \tau &= -hMv_{ref}\omega + (J+Mh^2)\ddot{\theta} \\ &\quad -(hMg + h^2M\omega_{ref}^2)\theta. \end{aligned} \tag{28}$$

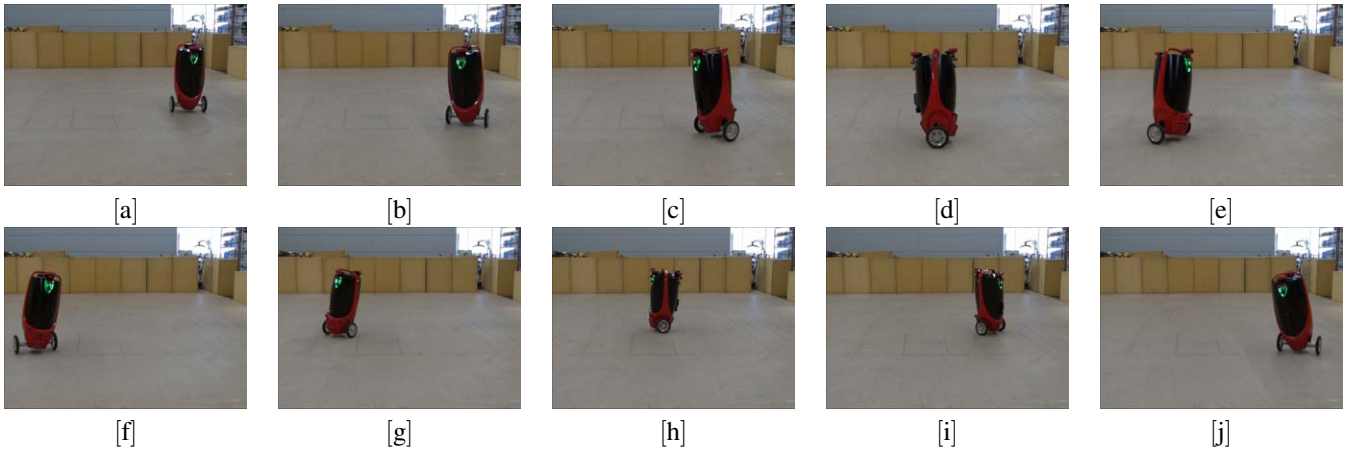

Fig. 9. Snapshots of turning motion in experiment.

In addition, the jerk j_x around the x axis can be shown as follows:

$$j_x = \ddot{\theta}[k] - \ddot{\theta}[k-1]. \tag{29}$$

B. Transformation of $V[k]$

$Z[k]$ can be given as follows:

$$\begin{aligned} Z[k] &= \begin{bmatrix} C & \dots & 0 \\ \vdots & \ddots & \vdots \\ 0 & \dots & C \end{bmatrix} \begin{bmatrix} \hat{X}[k+1|k] \\ \vdots \\ \hat{X}[k+N_p|k] \end{bmatrix}, \\ &= C_p X_p[k], \end{aligned} \tag{30}$$

where $X_p[k]$ can be shown as follows:

$$\begin{aligned} X_p[k] = &\begin{bmatrix} A \\ \vdots \\ A^{N_u} \\ A^{N_u+1} \\ \vdots \\ A^{N_p} \end{bmatrix} X[k] + \begin{bmatrix} B \\ \vdots \\ \sum_{i=0}^{N_u-1} A^i B \\ \sum_{i=0}^{N_u} A^i B \\ \vdots \\ \sum_{i=0}^{N_p-1} A^i B \end{bmatrix} u[k-1] \\ + &\begin{bmatrix} B & \dots & 0 \\ AB+B & \dots & 0 \\ \vdots & \ddots & \vdots \\ \sum_{i=0}^{N_u-1} A^i B & \dots & B \\ \sum_{i=0}^{N_u} A^i B & \dots & AB+B \\ \vdots & \vdots & \vdots \\ \sum_{i=0}^{N_p-1} A^i B & \dots & \sum_{i=0}^{N_p-N_u} A^i B \end{bmatrix} \Delta U[k]. \end{aligned} \tag{31}$$

By substituting (31) into (30), $Z[k]$ is redefined as follows:

$$Z[k] = \Phi X[k] + \Upsilon u[k-1] + \Theta \Delta U[k]. \tag{32}$$

By substituting (32) into $V[k]$ in (17), $V[k]$ can be modified into the following quadratic form:

$$\begin{aligned} V[k] = &\Delta U[k]^T (\Theta^T Q \Theta + W) \Delta U[k] \\ &-2\Delta U[k]^T \Theta^T Q E[k] + E[k]^T Q E[k], \end{aligned} \tag{33}$$

where $E[k]$ is shown as follows:

$$E[k] = R[k] - \Phi X[k] - \Upsilon u[k-1]. \tag{34}$$

C. Transformation of Inequalities

(18) and (19) can be modified as follows:

$$\begin{aligned} \begin{bmatrix} I_{N_p} \\ -I_{N_p} \end{bmatrix} Q_y[k] &\le \begin{bmatrix} q_{ymax} \\ q_{ymin} \end{bmatrix}, \\ \Gamma_q Q_y[k] &\le g_q, \end{aligned} \tag{35}$$

$$\begin{aligned} \begin{bmatrix} I_{N_p} \\ -I_{N_p} \end{bmatrix} T[k] &\le \begin{bmatrix} \tau_{max} \\ \tau_{min} \end{bmatrix}, \\ \Gamma_\tau T[k] &\le g_\tau, \end{aligned} \tag{36}$$

where I_{N_p} is the $N_p \times N_p$ unit matrix. $Q_y[k]$ and $T[k]$ can be extracted from $Z[k]$ and expressed as follows by using the correspondent matrices Φ_q, Φ_τ, Υ_q, Υ_τ, Θ_q, and Θ_τ:

$$Q_y[k] = \Phi_q X[k] + \Upsilon_q u[k-1] + \Theta_q \Delta U[k], \tag{37}$$

$$T[k] = \Phi_\tau X[k] + \Upsilon_\tau u[k-1] + \Theta_\tau \Delta U[k]. \tag{38}$$

By substituting (37) and (38) into (35) and (36), (35) and (36) can be transformed into the following linear inequalities of $\Delta U[k]$:

$$\begin{aligned} \Gamma_q \Theta_q \Delta U[k] \le &-\Gamma_q \Phi_q X[k] \\ &-\Gamma_q \Upsilon_q u[k-1] + g_q, \end{aligned} \tag{39}$$

$$\begin{aligned} \Gamma_\tau \Theta_\tau \Delta U[k] \le &-\Gamma_\tau \Phi_\tau X[k] \\ &-\Gamma_\tau \Upsilon_\tau u[k-1] + g_\tau \end{aligned} \tag{40}$$

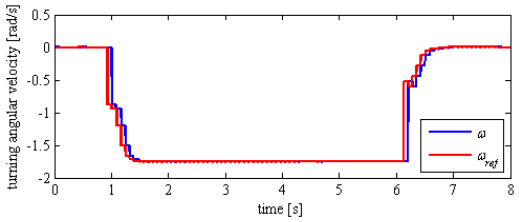

[a] turning angular velocity

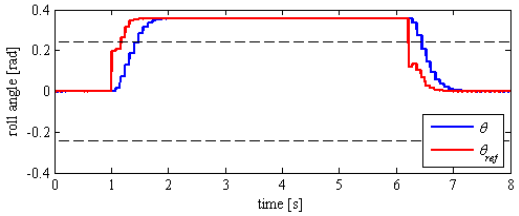

[b] roll angle

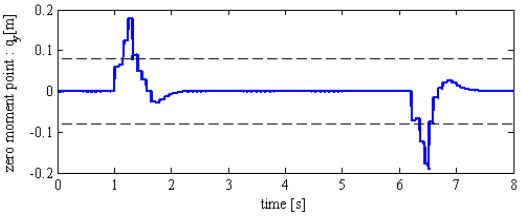

[c] zero moment point

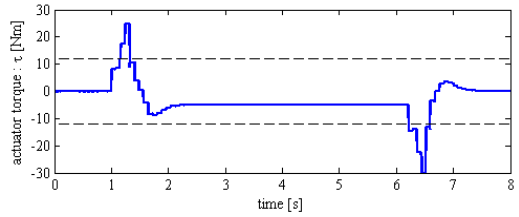

[d] actuator torque

Fig. 10. Simulation results for the conventional approach. (v_{ref} = 1.667 [m/s], ω_{refc} = 0.5886 [rad/s])

On the other hand, the following matrices are defined to modify (20):

$$\begin{aligned} F &= \left[\begin{array}{ccc} F_1 & \ldots & F_{N_u} \end{array}\right] = \left[\begin{array}{c} I_{N_u} M \\ -I_{N_u} M \end{array}\right], \\ f &= [\theta^T_{max}, \ -\theta^T_{min}]^T, \end{aligned} \tag{41}$$

where I_{N_u} is the $N_u \times N_u$ unit matrix, and M can be shown as follows:

$$M = \left[\begin{array}{cccc} m_{one} & 0 & \ldots & 0 \\ 0 & m_{one} & \ldots & 0 \\ \vdots & & \ddots & \vdots \\ 0 & 0 & \ldots & m_{one} \end{array}\right], \tag{42}$$

where $m_{one} = [1 \ \ 0]$. (20) can be transformed as follows:

$$F_y \Delta U(k) \leq -F_{x1} u[k-1] - f, \tag{43}$$

where F_y and F_{x1} can be shown as follows:

$$\begin{aligned} F_y &= [F_{x1}, \ \ldots \ F_{xN_u}], \\ F_{xi} &= \sum_{i=1}^{N_u} F_i. \end{aligned} \tag{44}$$

As a result, the inequalities (18), (19), and (20) can be modified as the linear inequalities of $\Delta U[k]$ to formulate the quadratic programming problem.

References

[1] M. Yamaoka, Personal Mobility Robot, Journal of the Robotics Society of Japan, Vol.26, No.8, pp.27–28, 2008.

[2] Y. Hosoda, S. Egawa, J. Tamamoto, K. Yamamoto, R. Nakamura, and M. Togami, Basic Design of Human-Symbiotic Robot EMIEW, Proc. of the 2006 IEEE/RSJ International Conference on Intelligent Robots and Systems, pp. 5079–5084, 2006.

[3] M. Morita, and A. Yanaka, "Personal Mobility i-REAL", Journal of Society of Automotive Engineers of Japan, Vol.66, No.12, pp.36–41, 2012.

[4] N. Hirose, R. Tajima, and K. Sukigara, Personal Robot Assisting Transportation to Support Active Human Life – Posture Stabilization based on Feedback Compensation of Lateral Acceleration, Proc. of the IEEE/RSJ International Conference on Intelligent Robots & Systems, pp.659–664, 2013.

[5] T. Takei, R. Imamura, and S. Yuta, Baggage Transportation and Navigation by a Wheeled Inverted Pendulum Mobile Robot, IEEE Trans. on Industrial Electronics, Vol. 56, No. 10, pp. 3985–3994, 2009.

[6] N. Hirose, R. Tajima, K. Sukigara, and Y. Tsusaka, Posture Stabilization for a Personal Mobility Robot using Feedback Compensation with an Unstable Pole, Proc. of IEEE International Conference on Mechatronics, pp.804–809, 2013.

[7] R. Rajamani, J. Gohl, L. Alexander, and P. Starr, Dynamics of Narrow Tilting Vehicle, Mathematical and Computer Modeling of Dynamical Systems, Vol.9, No.2, pp. 209–231, 2003.

[8] D. Piyabongkarn, T. Keviczky, and R. Rajamani, "Active Tilt Control for Stability Enhancement of a Narrow Commuter Vehicle", International Journal of Automotive Technology, Vol.5, No.2, pp. 77–88, 2004.

[9] M. Krid, and F. Benamar, Design and control of an active anti-roll system for a fast rover, Proc. of the 2011 IEEE/RSJ International Conference on Intelligent Robots and Systems, pp. 274–279, 2011.

[10] J. M. Maciejowski, Predictive Control with Constraints, Prentice Hall, 2000.

[11] P. B. Wieber, Trajectory Free Linear Model Predictive Control for Stable Walking in the Presence of Strong Perturbations, Proc. of the IEEE-RAS International Conference on Humanoid Robots, pp.137–142, 2006.

[12] S. Kajita, F. Kanehiro, K. Kaneko, K. Fujiwara, K. Harada, K. Yokoi, and H. Hirukawa, Biped Walking Pattern Generation by using Preview Control of Zero-Moment Point, Proc. of the IEEE International Conference on Robotics & Automation, pp. 1620–1626, 2003.

[13] A. Shimada, and N. Hatakeyama, High-Speed Motion Control of Wheeled Inverted Pendulum Robots, Proc. of 4th IEEE International Conference on Mechatronics, pp. 1–6, 2007.

[14] N. Hirose, K. Sukigara, H. Kajima, and M. Yamaoka, Mode Switching Control for a Personal Mobility Robot based on Initial Value Compensation, Proc. of the 36th Annual Conference of the IEEE Industrial Electronics Society, pp.1908–1913, 2010.

[15] M. Tanaka, R. Tajima, A. Fujii, Y. Tsusaka, N. Hirose, and K. Sukigara, Personal Robot to Support Active Human Life by Assisting Transportation – Person detection and following –, Proc. of JSME Robomec 2013, 2A2–Q02 (in Japanese).

[16] N. Hirose, M. Iwasaki, M. Kawafuku, and H. Hirai, Deadbeat Feedforward Compensation with Frequency Shaping in Fast and Precise Positioning, IEEE Trans. on Industrial Electronics, Vol. 56, No.10, pp. 3790 – 3797, 2009.

[17] N. L. Ricker, Model Predictive Control with State Estimation, Ind. Eng. Chem. Research, Vol.29, pp. 374–382, 1990.